ac conductivity, surface impedance:
experiments and applications...

Surface resistance: ω² dependence

$$T \ll T_c$$

$$R_S = \frac{\sigma_0 \mu_o^2 \lambda_L^2 \omega^2 f_n}{2}$$

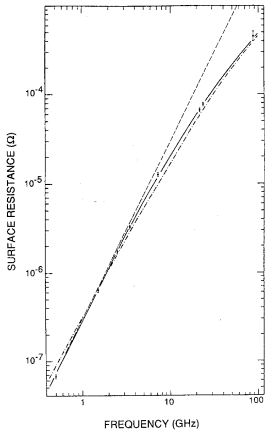

Fig. 5. The surface resistance of Nb at 4.2 K as a function of frequency [62,63]. Whereas the isotropic BCS surface resistance (– · – ·) resulted in $R \propto \omega^{1.8}$ around 1 GHz, the measurements fit better to ω^2 (– – –). The solid curve, which fits the data over the entire range, is a calculation based on the smearing of the BCS density-of-states singularity by the energy gap anisotropy in the presence of impurity scattering [61]. The authors thank G. Müller for providing this figure.

J. P. Turneaure, 1 J. Halbritter, z and H. A. Schwettman
J. Supercond. 4, 341 (1991)

Surface resistance: ω² dependence

$$T \ll T_c$$

$$R_S = \frac{\sigma_0 \mu_o^2 \lambda_L^2 \omega^2 f_n}{2}$$

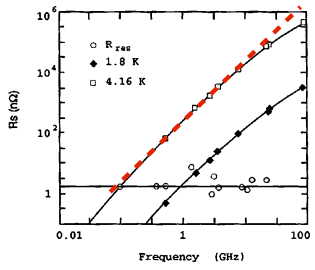

Figure 17. Frequency dependence of the surface resistance of Nb. Note the departure from a square law at high frequencies, indicative

H. Padamsee
Supercond. Sci. Technol. 14, R28 (2001)

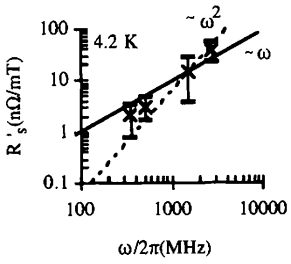

Figure 20. Q-slope for Nb/Cu cavities at various frequencies.

Surface resistance and the gap

$$T \ll T_c$$

$$R_S = \frac{\sigma_0 \mu_o^2 \lambda_L^2}{2} \omega^2 f_n$$

$$T \to 0$$

$$f_n^{\{BCS\}} \sim \sqrt{\frac{2\pi\Delta(0)}{k_B T}} e^{-\Delta(0)/k_B T}$$

(local limit, clean)

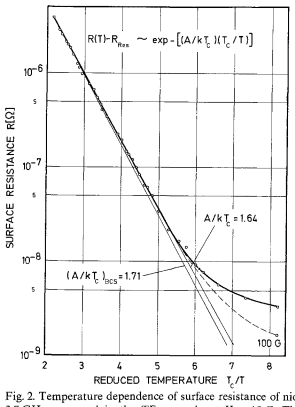

Fig. 2. Temperature dependence of surface resistance of niobium at 3.7 GHz measured in the TE_{011} mode at $H_{rf} \simeq 10$ G. The values computed with the BCS theory used the following material parameters:
$T_c = 9.25$ K; $\lambda_L(T=0, l=\infty) = 320$ Å;
$\Delta(0)/kT = 1.85$; $\xi_F(T=0, l=\infty) = 620$ Å; $l = 1000$ Å or 80 Å.
The measured $\Delta(0)/kT_c \simeq 1.78$ $(A/kT_c = 1.64)$ is smaller than for pure Nb, which indicates – together with the short mean free path of 80 Å – that a surface layer of Nb is enriched with interstitial 0

J. Halbritter
Z. Physik **266**, 209 (1974)

Enrico Silva - diritti riservati - Non è permessa, fra l'altro, l'inclusione anche parziale in altre opere senza il consenso scritto dell'autore

Surface resistance and the gap

$$T \ll T_c$$

$$R_S = \frac{\sigma_0 \mu_o^2 \lambda_L^2}{2} \omega^2 f_n$$

$$T \to 0$$

$$f_n^{\{BCS\}} \sim \sqrt{\frac{2\pi\Delta(0)}{k_B T}} e^{-\Delta(0)/k_B T}$$

(local limit, clean)

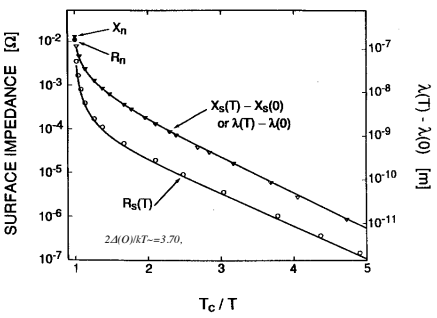

Fig. 3. The superconducting surface resistance $R_s(T)$ and the surface reactance $X_s(T) - X_s(0)$ [or $\lambda(T) - \lambda(0)$] as a function of temperature for Nb at 8.6 GHz. The surface resistance and reactance data are plotted with the symbols ○ and ▽, respectively. The solid curves are the surface resistance and the surface reactance calculated from the Mattis–Bardeen theory. R_n and X_n are the normal-state surface resistance and reactance measured just above T_c. The authors thank C. M. Lyneis for providing this data [53].

J. P. Turneaure, 1 J. Halbritter, z and H. A. Schwettman
J. Supercond. 4, 341 (1991)

Enrico Silva - diritti riservati - Non è permessa, fra l'altro, l'inclusione anche parziale in altre opere senza il consenso scritto dell'autore

Superfluid: λ

$$\lambda(T) = \frac{\lambda(0)}{(f_s(T))^{1/2}} = \frac{\lambda(0)}{[1 - f_n(T)]^{1/2}}$$

$$T \ll T_c \qquad f_n \ll 1$$

$$\lambda(T) \simeq \lambda(0)\left[1 + \frac{1}{2} f_n(T)\right]$$

$$T \to 0$$

$$f_n^{\{BCS\}} \sim \sqrt{\frac{2\pi\Delta(0)}{k_B T}} e^{-\Delta(0)/k_B T}$$

(local limit, clean)

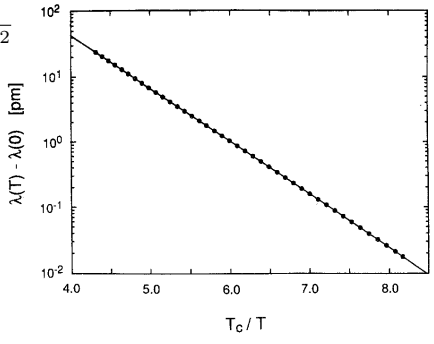

Fig. 4. The penetration depth change, $\lambda(T) - \lambda(0)$, as a function of temperature for Nb at 8.6 GHz for large values of T_c/T. The circles are measured data with a resolution at the lowest temperature of about 10^{-16} m. The solid curve is the best-fit function of the form $\exp(-\Delta(0)/kT)$ with $2\Delta(0)/kT_c = 3.736$, which for these data is an adequate approximation to the Mattis–Bardeen theory.

J. P. Turneaure, 1 J. Halbritter, z and H. A. Schwettman
J. Supercond. 4, 341 (1991)

Losses

Normal metal
(normal skin effect)

$$R_S = \sqrt{\frac{\omega\mu_0}{2\sigma}} \propto \omega^{1/2}$$

Superconductor

$$T \ll T_c$$

$$R_S = \frac{\sigma_0 \mu_o^2 \lambda_L^2}{2} \omega^2 f_n$$

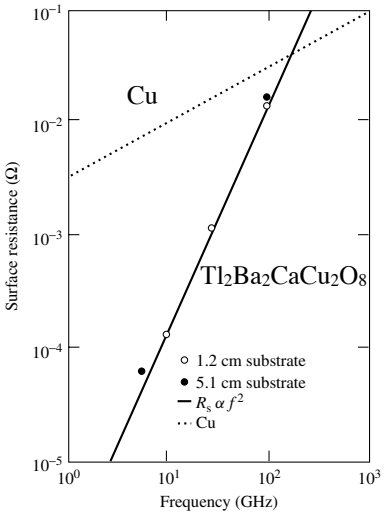

Losses

Normal metal
(normal skin effect)

$$R_S = \sqrt{\frac{\omega\mu_0}{2\sigma}} \propto \omega^{1/2}$$

Superconductor

$$T \ll T_c$$

$$R_S = \frac{\sigma_0 \mu_o^2 \lambda_L^2}{2} \omega^2 f_n$$

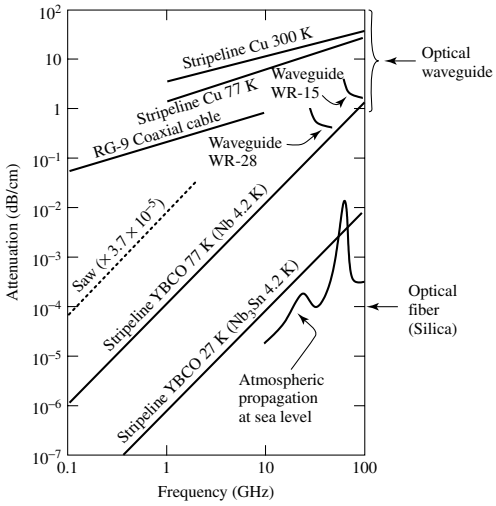

Applications: filters

Low losses: better filters!

better filters -> no
spurious harmonics.

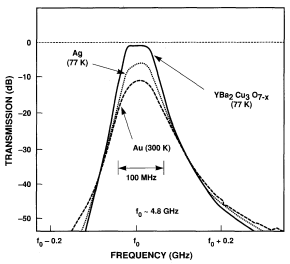

Fig. 15. Measured response at 77 K of the four-pole-Chebyshev 1% bandwidth YBCO microstrip filter shown in the previous figure. The measured response of the same filter fabricated from silver (operated at 77 K) and gold (operated at 300 K) are shown for comparison. The superconducting filter exhibits a dramatic improvement in insertion loss and filter shape factor. (From [163].)

N. Newman, W. G. Lyons
J. Supercond 6, 119 (1993)

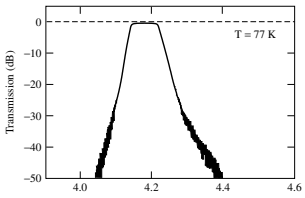

Figure 11.17 Measured transmission response at 77 K of a filter fabricated with a postannealed YBCO signal line and ground plane on a 425 µm thick $LaAlO_3$ substrate. Passband insertion loss is 0.3 dB. After Lyons and Withers [162].

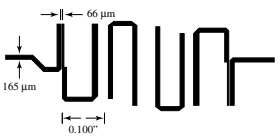

Figure 11.16 Four-pole superconductive microstrip filter layout. The filters were fabricated on $LaAlO_3$ substrates using gold, niobium and YBCO signal lines. After Lyons and Withers [162].

K. Fossheim, A. Sudbø, *"Superconductivity - Physics and applications"*, John Wiley and Sons, Ltd

Applications: filters

Low losses: better filters!

better filters -> no spurious harmonics.

Fig. 3. A view of an assembled LG HTS receiver front-end consisting of a 12-pole HTS filter, LNAs and a temperature-controlled cryocooler. Its specifications are listed in Table I.

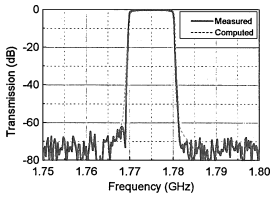

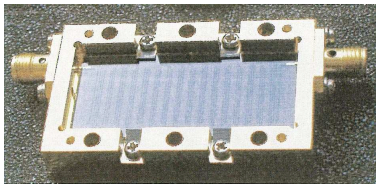

Fig. 2. (a) S_{21} data for the LG 16-pole YBCO filter at 70 K. The 16-pole filter has the same pass band and the center frequency as the 12-pole filter in Fig. 1. Increased number of poles resulted in improved out-band characteristics (40–50 dB/MHz) at the expense of insertion loss (~0.2 dB). The simulated results (dotted line) appear to match well with the measured ones after tuning; (b) A view of the packaged LG 16-pole YBCO filter. The dimensions of the substrate are $45 \times 18 \times 0.5$ mm^3.

S. Y. Lee and B. Oh
J. Supercond. 16, 823 (2003)

Applications: accelerating cavities

Low losses: high accelerating fields

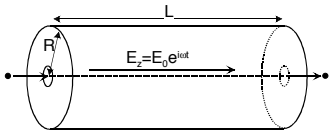

Fig. 7.26 Principle of the acceleration of charged particles in a cylindrical resonating cavity. The resonator is excited in the "TM_{010} mode", in which the electric field is oriented parallel to the z axis, and the magnetic field in azimuthal direction.

W. Buckel, R. Kleiner, "Superconductivity - Fundamentals and Applications" (Wiley)

LHC at CERN

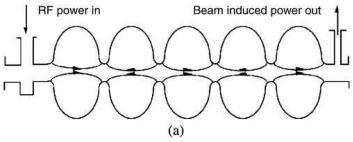

(a)

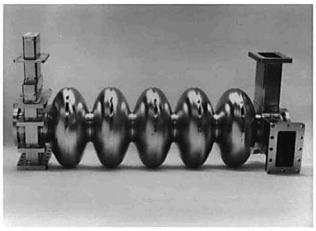

(b)

Fig. 7.27 Resonator structure for the acceleration of electrons at CEBAF (Jefferson Laboratory, Cornell, USA). Top: cross-sectional drawing. Bottom: real structure. The structure consists of five resonators covered with a Nb layer and placed in series. Its active length is 50 cm. The resonance frequency is 1.5 GHz. The electron beam traverses the resonator during one half-wave, whereas it traverses the opening between the resonators during the second half-wave. Therefore, within the resonators the electrons always experience an electric field that accelerates them in the forward direction. (From [70] with permission of IOP).

Applications: delay lines

Phase velocity:
(i) small
(ii) frequency independent

Compact delay lines (signal "waits" to be processed)
Dispersionless !

Ideal delay lines:
• lossless
• without dispersion (the signal does not "spread")

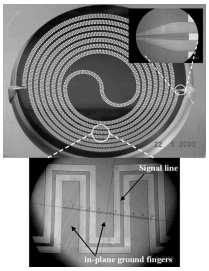

Hieng Tiong Su · Yi Wang · Frederick Huang · Michael J. Lancaster
J Supercond Nov Magn (2008) 21: 7–16

Fig. 1 Three examples of superconducting delay lines: **(a)** meander lines [16]; **(b)** double-spiral [2]; **(c)** unit-cell structure [17]; and **(d)** coplanar double-spiral meander lines [10]. The two insets show enlargement of the coplanar line taper transition and the coplanar meander line section